Taylor & Francis
Taylor & Francis Group

Vehicle System Dynamics
International Journal of Vehicle Mechanics and Mobility

ISSN: 0042-3114 (Print) 1744-5159 (Online) Journal homepage: www.tandfonline.com/journals/nvsd20

Tyre and brake thermal management in NASCAR

D.J.N. Limebeer, R.A. Dollar, S. Sivaramakrishnan & N. Gordhan

To cite this article: D.J.N. Limebeer, R.A. Dollar, S. Sivaramakrishnan & N. Gordhan (2025) Tyre and brake thermal management in NASCAR, Vehicle System Dynamics, 63:2, 398-423, DOI: 10.1080/00423114.2024.2342534

To link to this article: https://doi.org/10.1080/00423114.2024.2342534

Published online: 24 May 2024.

VEHICLE SYSTEM DYNAMICS
2025, VOL. 63, NO. 2, 398–423
https://doi.org/10.1080/00423114.2024.2342534

Tyre and brake thermal management in NASCAR

D.J.N. Limebeer[a], R.A. Dollar[b], S. Sivaramakrishnan[b] and N. Gordhan[a]

[a]School of Electrical and Information Engineering , University of the Witwatersrand, Johannesburg, South Africa; [b]General Motors (Motorsports), Charlotte Technical Center, Concord, NC, USA

ABSTRACT

The need to manage race car tyres is routine faire and several academic papers have already appeared on this topic. We contribute to this literature with refined tyre grip and wear-rate models. Less well known is a methodology for managing the thermal transients in the car's braking system. This knowledge gap is addressed with a physically-based disc-and-calliper brake-heating model. The parameters in each of the models are optimised against measurement data captured on an instrumented Generation 7 (Gen 7) NASCAR driven on the Darlington speedway. These models are replicated on each corner of the vehicle. The remainder of the paper is directed to studying the minimum lap time performance of a Gen 7 NASCAR that is subject to tyre wear and temperature variations; brake heating influences are emphasised. Due to their novelty, the results focus on the performance impact of temperature variations and constraints on the front brake disc temperatures. Constraints on the brake temperatures are introduced to protect the brakes from fade and thermally-induced damage.

ARTICLE HISTORY
Received 26 June 2023
Revised 12 February 2024
Accepted 4 April 2024

KEYWORDS
Thermal tyre model; tyre friction; tyre wear; brake heating; brake disc thermal modelling; optimal control; generation 7 NASCAR

1. Introduction

High-performance road vehicles require the management and dissipation of heat from a variety of sources. These include the engine, batteries, tyres, and brakes. If engines overheat they are likely to suffer damage that can be expensive to repair. The batteries in electric vehicles need to be cooled in order to conserve their performance and lifespan. The frictional performance of tyres degrades if they are not operated within an optimal band of temperature. Brake discs, that are typically made from cast iron, are subjected to high thermal stresses which can lead to permanent plastic deformation and cracking.

The handling performance of road vehicles depends on the interaction between the tyres' tread and the road. The efficacy of this force-generation process depends on the tyres' temperature, wear status and the contact conditions between the tyre tread and the road. While tyre tread wear and friction are separate phenomena, these performance criteria are closely related. Tyre-focussed research has shown that the friction-related properties of tyre rubber are complex and influenced by a number of factors including the tyre compound, track roughness, tyre loading, and the tread temperature [1]. Of particular import is the fact that tyre wear reduces the available friction, and consequently erodes the vehicle's long-stint race performance [2].

CONTACT D.J.N. Limebeer david.limebeer@eng.ox.ac.uk, david.limebeer@wits.ac.za

This paper addresses the thermal management of the tyres and brakes of Gen 7 NASCAR-specification vehicles, and demonstrates that tyre and brake heat transfer management can be enhanced by optimal control. The thermal management of the tyres builds on the work in [3–5], while the use of optimal control in brake and calliper cooling appears to be new. Tyre saving has been the focus of attention in Formula One for several years. This is done to maintain the grip properties of the tyres, and to gain a strategic advantage in terms of potential overtaking opportunities. Tyre saving, whilst optimising lap times, is an important element of competitive racing.

Since friction-based brakes generate a substantial amount of thermal energy in a short time, brake disc cooling is a topic worthy of study. Overheating can cause brake fade, judder, increased component wear, as well as thermal cracking and brake fluid vaporisation. Other parts of wheel and suspension can also be adversely affected by high brake-disc temperatures. Tyre and brake cooling rely on a combination of conductive, convective and radiative cooling. Each of these topics will be considered, modelled and incorporated into a full-vehicle-track optimal control code of the type described in [6–8].

1.1. Tyre friction and wear

Tyre friction and wear are both responsive to temperature, which motivates a thermodynamic model of the tyre thermal behaviour. It should perhaps be emphasised that the models developed here are purpose-build for optimal control studies, and should not be considered competitors of more complex finite-element models of the type considered in [2,9,10].

The temperature-dependence of rubber friction was investigated in the early seminal work of Grosch [11]. He identified two components of rubber friction, namely *adhesion* and *deformation*. The former involves molecular-level interactions that manifests on smooth surfaces at low speeds, while the latter relates to high-speed sliding on rough surfaces. Grosch identified the fact that variations in the friction coefficient with temperature follows the rubber's stress-strain frequency response. He also observed that a WLF type transformation [12], which induces a horizontal shift of the frequency response, could be used to encapsulate the temperature dependence of rubber friction. In this way the adhesive and hysteretic components of friction can be characterised by a single, frequency-dependent master curve. For 'rough' tracks the master curve typically shows two friction peaks. The first originates from interfacial adhesion and is the only source of friction on smooth surfaces. The second is due to the deformation of the rubber surface as the track asperities pass over it. The friction curves obtained on a smooth surface are similar for all the polymers tested, in that they are almost symmetrical around a single maximum. In line with Grosch's findings, Persson [13] developed a theory of rubber friction and contact mechanics that predicts the coefficient of friction as a function of the power spectral density of any random rough surface and its temperature, normal pressure and sliding speed.

In early theoretical work it was found that at moderate slip tyre abrasion is proportional to the square of the slip [14]; the abrasion rate was assumed proportional to the friction power of dissipation. In the original notation, the wear per unit distance travelled is given by

$$w = \gamma_0 \rho f s^2 \tag{1}$$

where γ_0 is a material constant describing the 'abradibility' of the tread material per unit energy dissipation, ρ is the resilience of the wheel and f is the tyre's cornering stiffness and s is the side-slip angle. In later work this relationship was tested experimentally for a number of tyres available at the time, and was found wanting [15]. It was hypothesised that the tread temperature and the slip dependence of the tread properties might account for the observed shortcomings. It was also argued that for a given tread and tyre carcass construction, ρ and f are largely independent of the tread compound. Attention was thus focussed on temperature-related variations in the abradibility γ . In the case of temperature variations, the abradibility was modified to

$$\gamma = \gamma_0(1 + \alpha(t_s - t_0)) \tag{2}$$

where t_s and t_0 are the tyre's tread temperature and a reference temperature respectively. The constant α is used to reflect the fact that the abradibility of the tyre is temperature dependent, and recognises the fact that the tyre slip angle increases with temperature.

It was also observed that the appearance of abrasion patterns on the tyres' surface produces an increased rate of abrasion, which motivated a further modification to

$$\gamma = \gamma_0(1 + \alpha(t_s - t_0) + \beta\lambda) \tag{3}$$

with the wear assumed proportional to the abrasion spacing λ; β is a temperature-independent material constant. For the tyres tested at the time, the wear theory for slipping wheels performed satisfactorily if account is taken of temperature and abrasion pattern effects [15]. Rubber abrasion is reviewed in [16]. This paper describes the influence of various rubber material properties on abrasion and wear, how abrasion is initiated, and the development of surface abrasion on sharp and blunt tracks. It is concluded that reasonable predictions of abrasion rate can be made for simple contact geometries. However, in the general case, ill-defined loading conditions still make the prediction of rubber wear problematic.

In more recent work [17], it was pointed out that the temperature dependence of wear and the friction (when rubber slides on a hard rough substrate at a fixed velocity) has the form shown in Figure 1. It is important to note that the friction reduces at high temperature when the tyre becomes 'rubbery'. The friction then increases and reaches a maximum in an 'optimal' band of temperatures. At low temperatures, the friction coefficient again decreases as the rubber moves into the brittle 'glassy' region. Wear increases at high and low temperature, where the friction coefficient is compromised.

During sliding at low and intermediate temperatures the road surface asperities exert repetitive shear stresses on the rubber, but this stress is by itself not enough to break the strong covalent bonds within the rubber. However, at higher temperatures, thermal fluctuations may begin to break some of these chemical bonds; especially if the rubber has already been stretched by external stresses. This stress-assisted thermally-activated bond-breaking gives rises to an increase in high-temperatures wear. As explained in [13], accelerated wear may also occur at low temperatures where the rubber behaves as a more brittle material, and where the rubber can fracture by crack propagation. This 'two-mechanism' theory of rubber abrasion [19] leads one to expect a U-shaped wear characteristic of the form illustrated in Figure 1. Important is the fact that wear is minimised at temperatures nearby those where the friction is maximised.

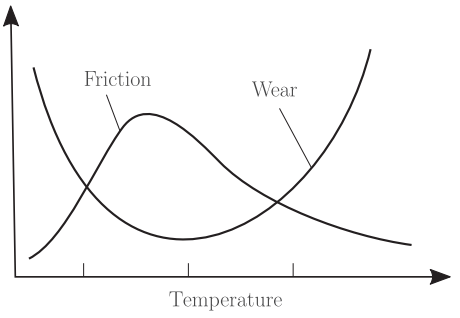

Figure 1. Temperature dependence of rubber friction and wear [13]; based on experimental results given in [18].

These well known properties of viscoelastic materials guide the modelling approach taken here, where two U-shaped curves (one inverted) will be used to represent the thermal properties of rubber friction and wear. The exact form of these curves is obviously dependent of the tyre's tread material.

1.2. Brake heating

The performance of a vehicle braking system can be degraded by excessive brake component temperatures–especially the brake discs. Rapid rises in the disc temperatures are produced by the transference of the car's kinetic energy into the sliding surface material of the brake pads and discs. Thermally-induced disc elastic deformation can result in several unwelcome problems including disc distortion, judder, squeal, run-out, and brake fade. Disc distortion can also alter the contact-pressure distribution that leads to thermal localisation such as hot-banding and hot-spotting; see Figure 2.

Finite element analysis is now the tool of choice that is used to predict the thermo-elastic behaviour of disc brakes [21]. Finite-element-based shape design optimisation is also being directed to the alleviation of these problems [20]. These computational advances have helped to reduce experimental testing and consequently development times and costs.

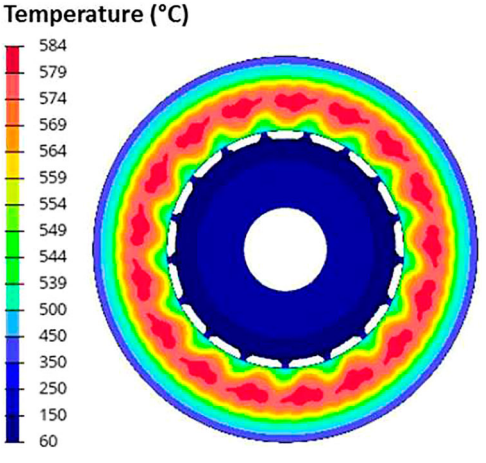

Figure 2. Simulated temperature distribution on the surface of a brake disc [20].

Most brake-related studies are based on finite-element solutions to a diffusion equation in combination with heat transfer interactions with the cooling air stream; see for example [20,22–25] and the references therein. In comparison, simpler lumped parameter treatments are relatively less well represented [26,27]. It is our purpose to develop such a model and then optimise its parameters.

During braking, every material point within the brake disc is subject to periodic heating; the temperature of each point can thus be expected to vary periodically. Due to the problem's symmetry, the temperature field is best described by a three-dimensional diffusion equation set up in cylindrical coordinates. In an unspun coordinate system, which is centred on the axis of the disc, the temperature field is $T(r,\theta,z,t)$; t is time, and r, θ and z are the spatial coordinates. The corresponding heat equation is

$$\frac{\partial^2 T}{\partial r^2}+\frac{1}{r}\frac{\partial T}{\partial r}+\frac{1}{r^2}\frac{\partial^2 T}{\partial \theta^2}+\frac{\partial^2 T}{\partial z^2}+Q=\frac{1}{k_p}\frac{\partial T}{\partial t}, \tag{4}$$

where Q is the (spatially-distributed) heat flow into the disc and k_p the disc material *thermal diffusivity*. After several revolutions of braking, the heat flow within the disc will be essentially constant in circumferential direction. This means that the temperature will be independent of θ, and the θ-dependent partial derivative terms are justifiably dropped.

In order to accommodate interactions with the environment, heating and cooling effects must be included as boundary conditions. These terms will include friction heating, diffusion terms that describe heat flows between interacting bodies, grey-body radiation losses to the environment, and diffusion and convection losses to the cooling air stream. These convection losses are particularly challenging to deal with, because they depends on several factors such as the transitions between laminar and turbulent flow regimes in the brake-ventilation air stream. These influences can only be studied with any fidelity with the aid of detailed CFD computations [25]. Consistent with the tyre-cooling model used here, we will develop a simple lumped-mass brake heating model suitable for use in vehicular optimal control studies.

Section 2 deals with modelling tyre tread and carcass temperatures, tyre wear modelling, and optimising the model parameters with measured data. Section 2.1 presents a simple method of representing the degradation of the tyre friction as a result of temperature variations, and the influence of the temperature on the tyre wear rate. Section 2.2 described the tyre thermal model used in this study. The tyre wear-rate model is presented in Section 2.2, with the results of a parameter optimisation study using measured track data given in Section 2.3. The lumped-parameter brake and calliper thermal models used here are described in Section 3, with the results of a parameter optimisation study presented in Section 3.1. Minimum lap time results appear in Section 4, with the conclusions presented in Section 5.

2. Quantitative representation of tyre heating

The friction and wear properties illustrated in Figure 1 must be quantified in order to properly represent the tyre being considered. If one has access to a list of measured data for example, one might approximate or interpolate this data using spline presentations for example. These spline representations could then be used to encode the curves in Figure 1 into an optimal control code. In this study we use two simple polynomial functions

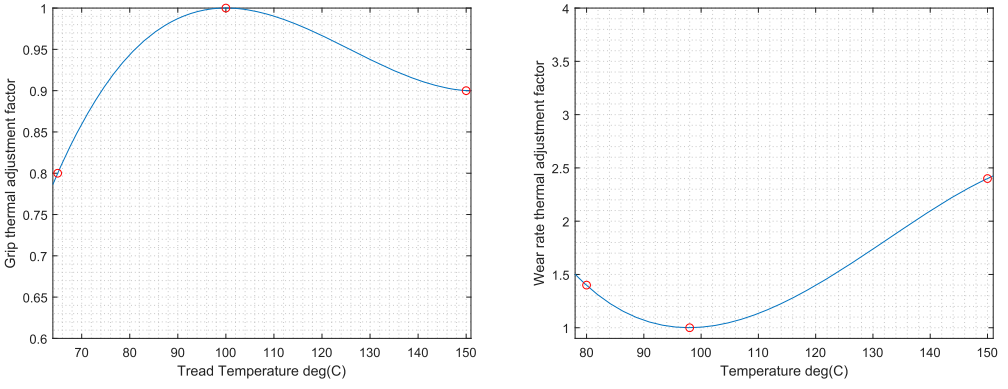

Figure 3. Quantitative dependence dependence of rubber friction and wear as a function of temperature. The grip cubic is illustrated in the A-part of the figure, while the wear-rate cubic is shown in the B-part of the figure.

of the tread temperature that are characterised by a small number of parameters, while recognising that other approaches would work equally well.

As is shown in Figure 3, the influence of the tread temperature on grip and wear rate are represented by a grip cubic $g(t)$ and a wear-rate cubic $w(t)$.

When setting up the optimal control problem three tyre grip and three tyre wear temperatures parameters values (the red circles in Figure 3) must be provided by the investigator. These parameter values must be informed by a knowledge of the tyre rubber properties being used. A fourth constraint comes from the fact that the gradients of $g(t)$ and $w(t)$ are set to zero at the optimal temperatures. It is assumed that:

(1) Both the grip and wear curves are unity at their optimal temperatures; see the minimum and maximum values in Figure 1;
(2) The derivatives of these curves are zero at their optima;
(3) Both the grip and wear functions are specified at values above and below the optimum temperatures.

Four constraints specify each of these functions; the two optimal temperatures are typically close together. Since cubic polynomials (and some other functions) can change sign, one must take care to ensure that these functions remain positive over the temperature range of interest.

Suppose that the grip polynomial in Figure 3 is described by

$$g(t) = at^3 + bt^2 + ct + d. \tag{5}$$

The optimal temperature t_{opt} constraint, its zero-gradient constraint, and the values of $g(t)$ above and below t_{opt} determine the four polynomial parameters as follows:

$$\begin{bmatrix} 1 \\ 0 \\ g(t_{low}) \\ g(t_{high}) \end{bmatrix} = \begin{bmatrix} t_{opt}^3 & t_{opt}^2 & t_{opt} & 1 \\ 3t_{opt}^2 & 2t_{opt} & 1 & 0 \\ t_{low}^3 & t_{low}^2 & t_{low} & 1 \\ t_{high}^3 & t_{high}^2 & t_{high} & 1 \end{bmatrix} \begin{bmatrix} a \\ b \\ c \\ d \end{bmatrix} \tag{6}$$

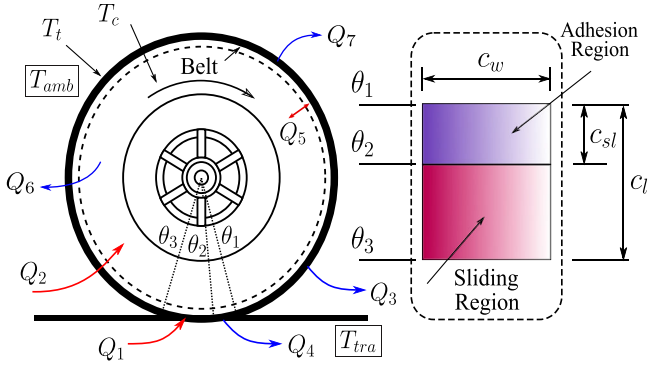

Figure 4. (Left) Dominant heat flows that determine the tyre's tread surface temperature T_t and its carcass temperature T_c. The angle θ_1 defines the angle at which ground contact is first made with the non-sliding region of the contact patch. The angle θ_2 defines the start of the sliding region, whilst θ_3 marks the end of ground contact. (Right) Plan view of the contact patch detailing its geometry; see [5].

$g(t_{low})$ and $g(t_{high})$ are given by the left- and right-hand red circles in Figure 3(A). These equations are easily solved by matrix inversion for the polynomial coefficients a, b, c and d provided t_{opt}, t_{low} and t_{high} are distinct. The wear-rate cubic $w(t)$ is dealt with in exactly the same way.

We will now present tyre thermodynamic and wear models with parameters that can then be optimised against measurement data. These models are used in quadruplicate–one for each wheel. The thermodynamic model uses five tunable parameters, while the wear model has two tunable parameters.

2.1. Tyre and tread thermal model

The tyre's thermodynamic model comprises two lumped masses, one representing the tyre's tread with (surface) temperature T_t and the other the tyre's carcass with bulk temperature T_c; see Figure 4.

The carcass temperature represents the temperature of the tyre's bulk material including the side-wall rubber, and the metal structure that provides the tyre with its basic shape and mechanical strength. The high thermal conductivity of the metal structure lends support to the isotropic thermal modelling assumption used here. The contact patch is divided into an adhesion region between angles θ_1 and θ_2, and a sliding region between angles θ_2 and θ_3. The ambient and track temperatures are designated T_{amb} and T_{tra}respectively (these values can be variable in space and time).

The earlier model in [5] is now modified to include different modelling assumptions as well as the inclusion of radiation heat loss terms. The differential equations for the tyre tread temperature, T_t, and the tyre carcass temperature, T_c, are described by simple heat-balance equations:

$$m_t c_t \dot{T}_t = Q_1 - Q_3 - Q_4 + Q_5 - Q_6 \tag{7}$$

$$m_c c_c \dot{T}_c = Q_2 - Q_5 - Q_7; \tag{8}$$

where m_t and m_c are the tread and carcass masses, while c_t and c_c are respectively the tread and carcass specific heat capacities. The tyre model comprises four temperatures and seven heat flows as detailed in Table 1.

Table 1. Tyre temperatures and heat flows.

Item	Description
T_t	Tread surface temperature
T_c	Carcass temperature
T_{amb}	Ambient air temperature
T_{tra}	Track surface temperature
Q_1	heat generated in the tyre sliding region
Q_2	heat generated due to tyre carcass deflection
Q_3	heat loss due to convective cooling
Q_4	conductive cooling in the adhesion region of the contact patch
Q_5	heat flow between the tread and the carcass
Q_6	radiation cooling from the tread surface
Q_7	radiation cooling from the tyre sidewall

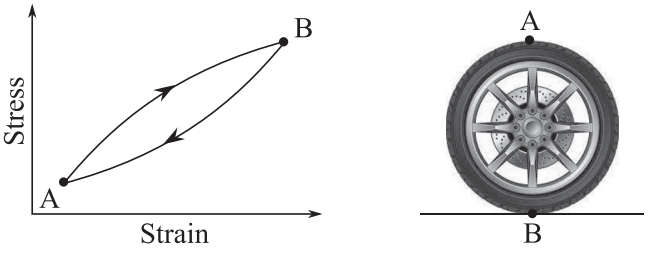

Figure 5. Hysteresis heating of the tyre carcass with the extreme points of stress-strain cycle.

We will assume that: (i) Q_1 is generated by tyre slip, (ii) Q_2 is generated by cyclic flexing of the tyre structural material and carcass, (iii) Q_3 is heat lost by convective cooling, (iv) Q_4 represents heat lost by conductive cooling in the adhesion region of the contact patch, (v) Q_5 represents the heat transfer between the tread and the carcass, (vi) the radiation cooling terms Q_6 and Q_7 are determined by the Stefan–Boltzmann law.

Following standard thinking [3–5], the heat generated in the contact patch is calculated by summing the longitudinal and lateral slip powers:

$$Q_1 = p_1 u_n (|F_x \kappa| + |F_y \tan \alpha|). \tag{9}$$

The tunable parameter p_1 represents the portion of frictional power that goes to heating the tread. In this study slip quantities α and κ, and the tyre forces F_x and F_y are either measured, or are calculated using standard formulae [6].

As the wheels rotate, the carcass undergoes cyclic loading and unloading, which causes the carcass to heat up [28]. This type of heat-generation information can be obtained by direct measurement; see Figure 2 in [9]. Figure 5 shows the stress-strain cycle along with the extreme points A and B.

For a given material, the work done per cycle per unit mass, ΔE, corresponds to the area under the hysteresis curve; ΔE is generally a nonlinear function of the temperature and the inflation-induced initial stress. If the dynamic rolling diameter is D, the mass of the tyre carcass is m_c, and the vehicle's longitudinal speed component is u_n, the heating power is of the form $Q_2 = f m_c \Delta E$, where $f = u_n/(\pi D)$ is the carcass material cycling frequency. Since the heating process is anisotropic, the tyre carcass deflection heating is represented by

$$Q_2 = \frac{u_n m_c}{\pi D} \left(p_2 |F_x| + p_3 |F_y| + p_4 |F_z| \right), \tag{10}$$

Table 2. Contact patch length parameters.

Parameter	p_{cp1}	p_{cp2}
right-front	0.0004437	0.681758
left-front	0.0099999	0.379096
right-rear	0.0001508	0.795321
left-rear	0.0099996	0.374554

in which p_2, p_3 and p_4 are optimisable parameters; separate parameters are used so that the anisotropic character of the tyre's construction can be captured.

The heat loss due to convection between the tyre tread and the surrounding ambient air is given by:

$$Q_3 = h_{forc} A_{conv} (T_t - T_{amb}), \tag{11}$$

where

$$A_{conv} = A_{tot} - c_w c_l \tag{12}$$

is the area accessible to the ambient air flow. The first term on the right-hand side of (12) is the total surface area of the tread

$$A_{tot} = \pi DW; \tag{13}$$

$W > c_w$ is the tyre width. The second term is the area of the tread in contact with the road–c_l and c_w are the length and width, respectively, of the contact patch; see Figure 4.

The length of the contact patch of each tyre can be calculated either by an empirical power-law formula such as

$$c_l = p_{cp1} |F_z|^{p_{cp2}}, \tag{14}$$

where p_{cp1} and p_{cp2} are tunable parameters, or using the geometry associated with the unloaded and rolling tyre radii. If each tyre rolling radius r_r is measurable, one might argue that $c_l = 2\sqrt{r_0^2 - r_r^2}$, where r_0 and r_r are the unloaded and rolling radii respectively. The parameters p_{cp1} and p_{cp2} can be fitted to measured loaded wheel radii data using a quadratic cost and a nonlinear programming algorithm such as fmincon MATLAB ®. The parameters in Table 2 where fitted to measured rolling radius data.

The heat transfer coefficient h_{forc} is determined using an empirical formula that correlates well with CFD simulation ([9] Equation 10):

$$h_{forc} = \frac{K_{air}}{L} \left[0.0239 \left(\frac{u_n L}{\nu_{air}} \right)^{0.805} \right]. \tag{15}$$

The conductivity and kinematic viscosity of air, are K_{air} and ν_{air} respectively, and are evaluated at the average temperature between the tread and ambient air. Numerical values can be found in material physical property databases–see for example Table A–9 [29]. The characteristic length of the heat exchange surface is given by:

$$L = \frac{1}{1/D + 1/W}, \tag{16}$$

where D is the tyre diameter and W the tread width.

Table 3. Thermodynamic model parameters.

Parameter	Description	Units	Value
m_t	Tyre tread mass	kg	0.9
m_c	Tyre carcass mass	kg	11.0
c_t	Heat capacity of tread	kJ/kg K	0.9
c_c	Heat capacity of carcass	kJ/kg K	1.6
h_{tt}	Track-tyre heat transfer coefficient	kW/m^{2}K	1.2
c_w	Contact patch width	m	0.2286
a_{cp}	Contact patch length constant	m/kN	0.056
α_c	Reference sliding/non-sliding slip angle	$^\circ$	8
c_{s1}	Sliding/non-sliding reference 1	–	0.3
c_{s2}	Sliding/non-sliding reference 2	–	0.8
r_0	unloaded tyre radius	m	0.3613
r_r	rolling radius	m	$\leq r_0$
r_{rim}	wheel-rim radius	m	0.229
D	Unloaded tyre diameter	m	0.4572
W	Tyre width	m	0.2921
ϵ	Emissivity of rubber	–	0.93
σ	Stefan–Boltzmann constant	W/m^2 K^4	5.67×10^{-8}

The conductive heat loss from the tyre tread to the track is given by Newton's law of cooling:

$$Q_4 = h_{tt} A_{cp} (T_t - T_{tra}), \tag{17}$$

where h_{tt} is the transfer coefficient of conduction between the track and the tread [3]. The non-sliding area of the contact patch A_{cp} is the given by:

$$A_{cp} = c_w c_s(\alpha) c_l, \tag{18}$$

where $c_s(\alpha)$ gives the proportion of the contact patch that is in the non-sliding region of the tread as the vehicle approaches its cornering limit (see Figure 4). In particular,

$$c_s(\alpha) = \frac{\alpha}{\alpha_c}(c_{s2} - c_{s1}) + c_{s1}, \tag{19}$$

where c_{s1} and c_{s2} are reference values given in Table 3; α_c is the reference slip angle.

The heat transfer between the tread and carcass is given by:

$$Q_5 = p_5 A_{tot} (T_c - T_t), \tag{20}$$

where p_3 is a tunable conduction heat transfer coefficient; A_{tot} is given in (13).

The radiation cooling terms are given by the Stefan–Boltzmann law:

$$Q_6 = \epsilon\sigma \left(\pi DW - A_{cp}\right) \left(T_t^4 - T_{amb}^4\right) \tag{21}$$

$$Q_7 = \epsilon\sigma \left(2\pi \left(r_0^2 - r_{rim}^2\right)\right) \left(T_c^4 - T_{amb}^4\right), \tag{22}$$

where ϵ is the emissivity of rubber, σ is the Stefan–Boltzmann constant, the bracketed quantities are the appropriate radiation surface areas, while T_t, T_c and T_{amb} given in degrees Kelvin. Several of the parameters relevant to the thermal dynamic model are given in Table 3.

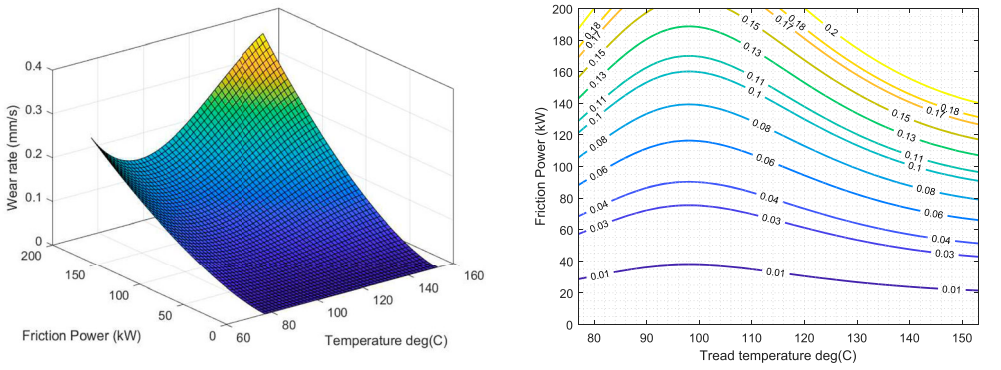

Figure 6. (A) Tyre wear rate as a function of the tread temperature and the friction power. (B) Wear rate contours as a function of tread temperature and the friction power generated in the contact patch.

2.2. Optimisable wear model

The tyre wear rate is described by the power law

$$\dot{w} = w_{p1} w(t) \left(\frac{Q_1}{Q_{ref}} \right)^{w_{p2}}, \tag{23}$$

in which Q_1 is the friction power generated in the tyre's contact patch (see (9)), Q_{ref} is a power reference, with w_{p1} and w_{p2} are tunable parameters. When $w(t) = 1$, the wear rate is determined by the optimal wear-rate temperature. When the temperature varies away from the optimal wear-rate temperature, the wear rate increases according to $w(t)$. This type of power law has been validated by experimentation and is now widely accepted as being structurally representative [17,30–33].

Figure 6 shows how tyre wear increases at high and low tread temperature, and increased friction power. This figure was generated by (23) using representative parameter values.

Figure 7(A) is representative of how a racing car tyre's grip varies throughout its life [1]. With the aid of this curve and Figure 3(A), one can generate Figure 7(B), which shows how tyre grip factor varies with temperature and the state of wear. Figure 7(A) is the curve of intersection between the grip-factor surface and the vertical plane at the tyre's optimal operating temperature.

2.3. Numerical calculations

The parameters in the tyre thermodynamic and wear models were optimised using measured data from tests on a Gen 7 NASCAR-specification vehicle. The left-side tires are physically different from the right-side tires. Each corner of the car has its own tyre thermal and wear parameters, but the same underlying generic model is used. The measurements that will be used in the opimisation process include: the tyre forces, the tyre rolling radii, the tyre carcass and tread temperatures, the tyre slip angles and slip ratios, tyre wear, and the track and ambient air temperatures. This data was acquired as follows:

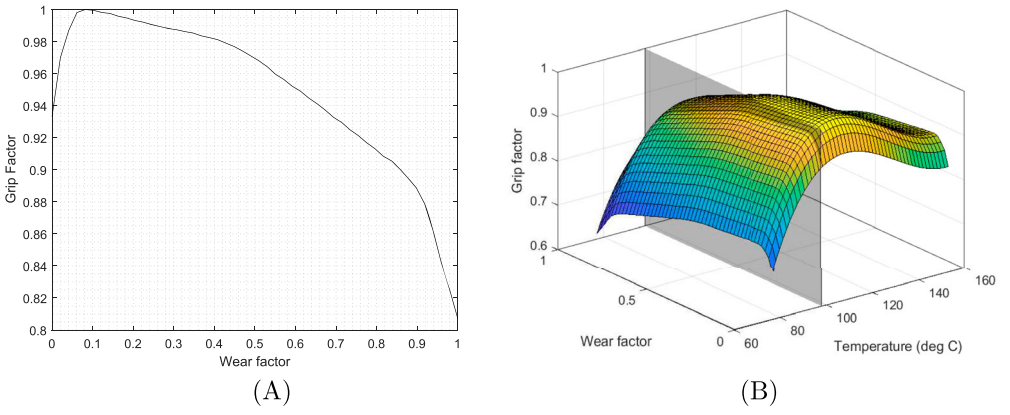

Figure 7. (A) Tyre grip as a function of wear at the optimal operating temperature (98°C). (B) Tyre grip factor as a function of wear and temperature.

- Tyre forces were measured using rims fitted with wheel force transducers (WFT) designed for motorsport applications. The WFT transducers measure the forces and moments at the interface between the wheel and the vehicle hub, and are expressed in the wheel-hub reference frame. These measurements are then transformed to the contact patch.
- The wheel rolling radii are calculated using an in-house model that has normal load, inflation pressure, vehicle speed and wheel camber as inputs. The model parameters were fitted to data measured with a MTS Flat-Trac^{R} tyre test system.
- The tyre velocity relative to the road is measured using optical sensors.
- Infrared sensors (IR) in the wheel rim are used to measure internal air and liner temperatures at multiple points along the width of the tyre. Additional sensors measure the tyre tread temperature at eight lateral locations.
- Wear is measured by taking tyre depth measurements at five locations laterally across the tyre tread (outer, mid-outer mid mid-inner and inner) at the end of the stint.

These measured quantities were then used evaluate the heats flows in Equations (9), (10), (11), (17), (20), (21) and (22). With these heat flows in place, the differential Equations (7) and (8) are solved for the tread and carcass temperatures respectively. The parameters p_1 to p_5 are optimise to minimise the integral-square errors between the modelled and measured tread and carcass temperatures. The wear parameters w_{p1} and w_{p2} in (23) were optimised so that measured end-of-lap wear measurements were obtained. The tyre wear was measured after a thirty-lap test stint. The per-lap wear target we used in our optimisation problem was one thirtieth of the mid-tread measured value. The measured change in tread depth after the test stint for the rear-right tyre was 0.9906 mm. We then assumed even wear for each lap which gives $0.9906/30 = 0.03302$ mm of wear per lap, which was the optimisation process target value. The other tyres were analysed in the same way.

The optimised parameter values for lap 15 were computed (this lap is representative of mid-stint operation). Figure 8 shows comparisons between the modelled and measured

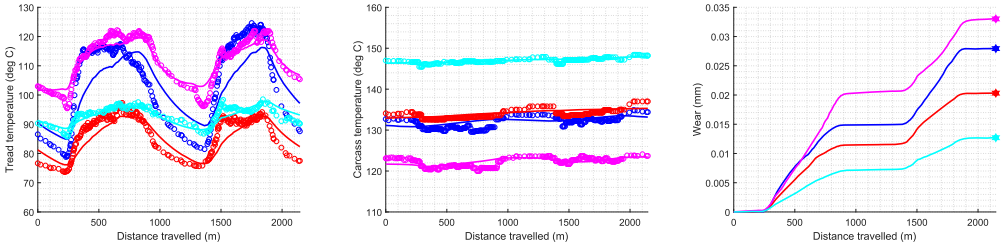

Figure 8. Tyre thermal and wear model parameter optimisation for lap 15 data. The measured data is shown in circles for temperature and stars for wear. The right-front is shown blue, the left-front red, the right-rear magenta, and the left-rear cyan.

Table 4. Optimised thermodynamic and wear model parameters for lap 15. The right-most columns show the RMS carcass and tread temperature estimation errors.

Parameter	p_1	p_2	p_3	p_4	p_5	w_{p_1}	w_{p2}	CT error	TT error
right-front	0.284	7.44e−05	1.345e−05	0.0013	150.7	1.225e−06	1.031	1.243°C	7.731°C
left-front	0.243	1.37e−05	6.977e−06	0.0039	111.8	2.655e−06	1.288	0.854°C	3.676°C
right-rear	0.328	0.0042	1.641e−05	1.797e−05	427.5	5.506e−06	1.785	0.955°C	2.044°C
left-rear	0.173	0.0038	0.0004	0.0013	166.5	4.051e−06	1.551	0.405°C	1.545°C

tread and carcass temperatures for all four tyres for lap 15. The tyre wear progression is shown in the right-hand plot, with the measured target values shown as stars.

The parameter values and RMS temperature errors for each test are shown in Table 4.

Aside from the right-front tread temperature, the correspondence between the measured values and the models' predictions with optimised parameter are good.

3. Brake thermal model

The braking system on most race cars comprises front and rear disc brakes that are fitted with ducted cooling. Ventilated discs are used to improve the heat transfer from the brake discs and callipers to the cooling airstream. The brake ducts typically channel air from the front of the car to each brake disc and are critical to maximising the performance and longevity of the braking system.

As opposed to using a diffusion equation such as (4), which treats the disc temperature as a scalar field, we propose to use a lumped-mass thermal model. In lumped mass models there is no need to consider spatially distributed heat sources and sinks, or temperature fields.

Figure 9 suggests that a lumped-mass model should include a thermal mass representing the disc, and a second representing the pad-calliper assembly.

The disc surface temperature is denoted T_d, while the pad-calliper assembly has temperature T_c. It is important to note that these temperatures correspond to isolated surface measurement points. This model is clearly inadequate for the study of phenomena such as thermal distortion induced by thermoelastic instabilities. Phenomena of this type are intimately related to temperature gradients within the brake disc material and must be studied using finite-element solutions to the diffusion Equation (4) [34].

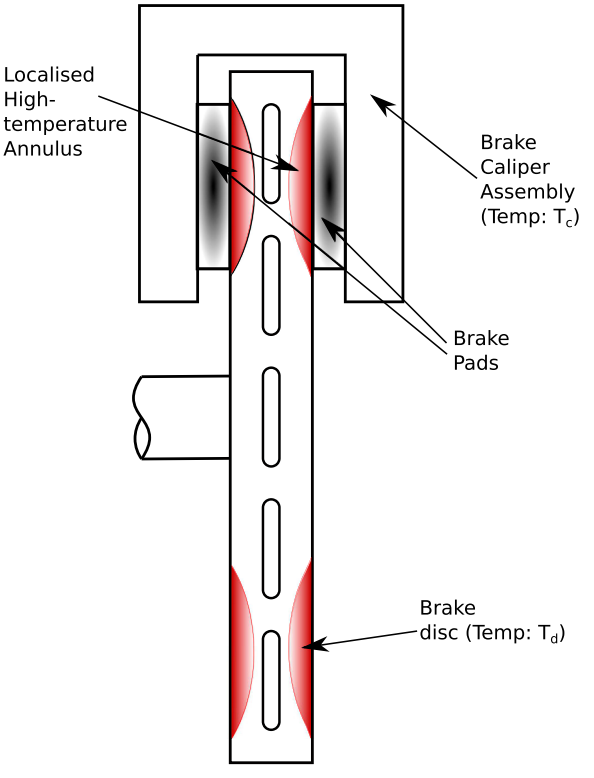

Figure 9. Two thermal-mass model of a NASCAR braking assembly. The disc has surface temperature T_d with the pad and calliper combination assigned surface temperature T_c.

Preceding as before, the temperatures of the disc and calliper-pad assembly are described by

$$\xi m_d c_d \dot{T}_d = \gamma Q_1 - Q_2 - Q_3 - Q_4 \tag{24}$$

$$m_c c_c \dot{T}_c = (1-\gamma)Q_1 + Q_2 - Q_5 - Q_6. \tag{25}$$

In (24) m_d and c_d are the mass and specific heat capacity of the disc. In order to better represent the transient surface temperature of the brake disc material, we introduce a mass participation factor ξ. Under firm braking the car's kinetic energy is rapidly converted into heat that manifests at the interface between the brake pads and discs and heats the tyres. Temperature T_d is used to represent the shallow annular fraction of the disc material that experiences extreme localised transient heating; see the red region of the left-hand side of Figure 9. It is this material that is being represented in (24). The main body of the disc will heat more slowly relying on longer time-scale diffusion. Variables $0 \leq \gamma \leq 1$ and Q_1 are, respectively, the heat participation ratio between the disc and calliper assembly and the friction heating power. In our model ξ and the heat participation ratio between the disc and calliper assembly will be treated as optimisable parameters. The heat flows Q_2, Q_3 and Q_4 represent, respectively, the heat conduction power flow from the disc to the calliper assembly, the convective heat loss to the cooling air stream and radiation heat loss from the surface of the discs.

Equation (25) is used to compute the temperatures of the brake callipers. Parameters m_c and c_c are the mass and specific heat capacity of the calliper assembly, with Q_5 and

Q_6 the convective heat loss from the calliper assembly to the cooling air stream, and the calliper assembly radiation cooling, respectively. The calliper assembly tends to heat and cool more slowly than the disc-surface material, and so no mass participation factor has been included.

The heat power supplied to the braking assembly given by

$$Q_1 = u_n \max(-F_x, 0), \tag{26}$$

where as before u_n is the vehicle speed and F_x is the longitudinal tyre force; the maximum function is used to recognise only longitudinal braking forces[1].

The heat transfer between the disc and calliper assembly is described by

$$Q_2 = 2k_p \frac{A_{pad}}{l}(T_d - T_c), \tag{27}$$

where k_p is the thermal conductivity of the brake pad material, A_{pad} is the pad surface area and l is the brake pad thickness. The Q_3 and Q_5 terms describe the radiation cooling of the disc and calliper assembly respectively, and are given by

$$Q_3 = \epsilon_d \sigma A_{disc}(T_d^4 - T_0^4) \tag{28}$$

$$Q_5 = \epsilon_c \sigma A_{cal}(T_c^4 - T_0^4), \tag{29}$$

where ϵ_d and ϵ_c are the emissivity of the disc and calliper assemblies, σ is the Stefan–Boltzmann constant, A_{disc} and A_{cal} are the radiative surface areas of the disc and calliper assemblies. The temperatures T_d, T_c and T_0 are the disc, calliper and the cooling air temperatures, respectively, in degrees Kelvin.

The most demanding modelling challenge comes from Q_4 and Q_6, which describe the conductive and convective heat transfers to the ducted brake-cooling air stream. In broad terms, these heat flows are described by

$$Q_4 = A_{disc}^{air} \alpha_{disc}(T_d, u_n)(T_d - T_0) \tag{30}$$

$$Q_6 = A_{cal}^{air} \alpha_{cal}(T_c, u_n)(T_c - T_0), \tag{31}$$

where A_{disc}^{air} and A_{cal}^{air} are the disc and calliper surface areas exposed to the cooling air stream, with $\alpha_{disc}(T_d, u_n)$ and $\alpha_{cal}(T_d, u_n)$ the corresponding heat transfer coefficients. A particular challenge is that the $\alpha(\cdot, \cdot)$s are functions of both the vehicle speed (u_n) and the disc (T_d) and calliper (T_c) surface temperatures.

The heat transfer from a rotating disk to an air stream parallel to the plane of rotation is studied in [25]. This is a 3D non-axisymmetric flow problem; See Figure 10.

The disk is assumed to have radius R and thickness d (assumed 'thin'), and rotates in the x, y-plane. The crossflow air stream has constant mean velocity u_{in}, with the disk rotating with angular velocity $\mathbf{\Omega}$. Far from the disk, the air's velocity field is assumed to be in the x-direction only. The disk surface temperature is assumed constant.

Before looking further at this study, we note that there are four assumptions that are not compatible with the brake cooling application: (i) the crossflow does not have a constant mean velocity, (ii) the disc's angular velocity is not constant, (iii) the disc cannot be assumed 'thin', and (iv) the disc surface temperature is not constant. As explained by a cited author in relation to experimental work [25]: 'it is likely that the nose of the disk used was disturbing the airflow as it was blunter than the profiles used by previous researchers

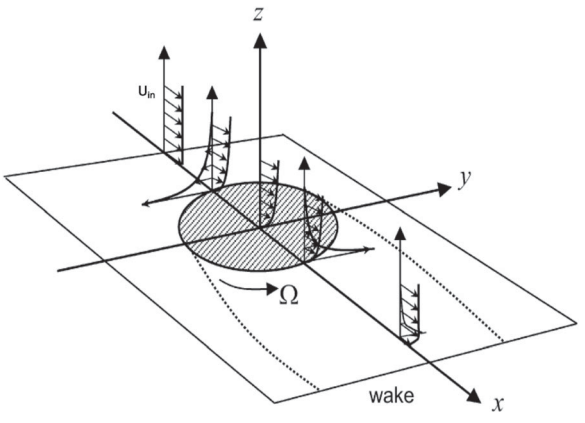

Figure 10. Spinning disc in a parallel crossflow [25].

to maintain laminar flow over a flat plate'. It is also worth mentioning that A_{disc}^{air} and A_{cal}^{air} cannot be treated as constant due to possible flow separation.

As detailed in [25], when the disc angular velocity is sufficiently high, asymmetric flow separation occurs that destroys the symmetry between the (co-moving) side and the (counter-moving) sides of the flow field. At lower disc angular velocities, when symmetric cooling occurs, the average heat transfer is essentially unaltered by the disc's rotational movement.

Setting aside any reservations associated with the idealizations and limitations assumed in the analysis, the study in [25] concluded that there is a critical ratio between the rotational and the crossflow Reynolds numbers below which there is no heat transfer augmentation due to spinning (relative to the non-spinning case). Put another way, 'if the disc doesn't spin fast enough, it can be treated as stationary from a heat transfer augmentation perspective.' In our application the cross flow and rotational Reynolds numbers are coupled, with the ratio of the rotational and crossflow Reynolds numbers small, which means that any heat transfer augmentation due to spinning is likely to be small. The question of disc surface temperature variations was not addressed in [25].

Given the aforementioned difficulties, a pragmatic approach is to suppose that $A_{disc}^{air}\alpha_{disc}(T_d, u_n)$ and $A_{cal}^{air}\alpha_{cal}(T_c, u_n)$ are non-negative polynomials in u_n and the associated disc and calliper surface temperatures[2]. This restriction ensures that the heat transfer coefficients remain non-negative for all u_n, T_d and T_c, thereby enforcing compliance with the second law of thermodynamics. Setting

$$A_{disc}^{air}\alpha_{disc}(T_d, u_n) = \begin{bmatrix} 1 & u_n & T_d \end{bmatrix} Q \begin{bmatrix} 1 \\ u_n \\ T_d \end{bmatrix} \tag{32}$$

$$= \begin{bmatrix} 1 & u_n & T_d \end{bmatrix} \begin{bmatrix} p_1 & \frac{p_2}{2} & \frac{p_3}{2} \\ \frac{p_2}{2} & p_4 & \frac{p_5}{2} \\ \frac{p_3}{2} & \frac{p_5}{2} & p_6 \end{bmatrix} \begin{bmatrix} 1 \\ u_n \\ T_d \end{bmatrix} \tag{33}$$

$$= p_1 + p_2 u_n + p_3 T_d + p_4 u_n^2 + p_5 u_n T_d + p_6 T_d^2, \tag{34}$$

Table 5. Brake assembly materials data.

Item	Value	Units
Disc Specific Heat Capacity	480.0	J/(kg-K)
Mass participation factor	0.1	–
Calliper Thermal Capacity	921.10	J/(kg-K)
Dics Mass (front)	8.8	kg
Dics Mass (rear)	4.9	kg
Calliper Mass (front)	5.0312	kg
Calliper Mass (rear)	3.274	kg
Disc Diameter (front)	380	mm
Disc Diameter (rear)	355	mm
Disc Mounting hole (front)	180	mm
Disc Mounting hole (rear)	210	mm
Disc Thickness (front)	36	mm
Disc Thickness (rear)	28	mm
Disc Surface Area (front)	0.6302	m^2
Disc Surface Area (rear)	0.5883	m^2
Pad Area (front)	9472	mm^2
Pad Area (rear)	6164	mm^2
Pad Thickness	25	mm
Pad Thermal Conductivity*	0.5	$W/(m\,K^\circ)$
Emissivity (Oxidised Aluminium)	0.25	–
Emissivity (Steel)	0.48	–
Stefan–Boltzmann constant	5.6704×10^{-8}	$(W/(m^2 \times K^4)$
Radiative Area calliper (front)	12.81	cm^2
Radiative Area calliper (rear)	7.87	cm^2

Note: *Several values have appeared in the literature. See for example [21,35,36].

it follows that $A_{disc}^{air}\alpha_{disc}(T_d, u_n)$ is non-negative if $Q \geq 0$. To simplify the non-negativity testing process, one can enforce $Q > 0$ by ensuring that the *leading* principal minors are positive. That is:

$$p_1 > 0$$
$$4p_1p_4 - p_2^2 > 0$$
$$4p_1p_4p_6 + p_2p_3p_5 - p_2^2p_6 - p_1p_5^2 - p_3^2p_4 > 0.$$

By considering permutations of rows and columns of Q, the positivity of any nested sequence of principal minors of Q is equivalent to Q being positive-definite. The heat transfer from the calliper assembly can be treated in much the same way using a further six parameters.

3.1. Numerical results

The results associated with the optimisation of the brake participation ratio γ appearing in (24) and (25), ξ appearing in (24), and the twelve parameters associated with the conductive and convection heat-loss modelling in (34) are now presented. These parameters were optimised to reproduce the disc and calliper temperature measurements taken from a Gen 7 NASCAR under race testing conditions. This study makes use of the disc and calliper assembly thermal parameters given in Table 5. In order to optimise the brake-calliper parameter set, we make use of surface temperature measurements made using infrared sensors mounted near the brake callipers.

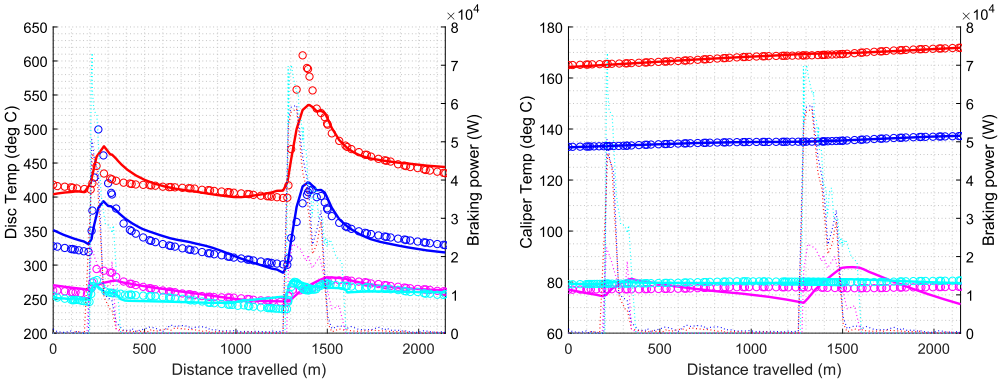

Figure 11. Disc (left) and calliper (right) thermal model parameter optimisation for lap 15 data. The measured data is shown in circles. The right-front is shown in blue, the left-front in red, the right-rear in magenta, and the left-rear in cyan. The feint dotted curves show the braking power for each wheel (see right-hand axis).

The need to optimise the mass participation factor ξ in (24) follows from the lump-parameter modelling assumption, that treats the disc temperature as being uniform. This is plainly untrue; see for example Figure 2. Under heavy braking, there is an annulus of disc material near the surface of the disc that appears periodically under the pads, which heat up significantly faster and to a higher temperature than the bulk of the disc material. The disc's outer peripheries heat up more slowly under the influence of thermal diffusion. While studies like that presented in [20] use realistic values for the disc mass and specific heat capacity, there are a number of important differences associated with this study. These include the facts that: (i) their simulations are based on solutions to the diffusion equation, (ii) the angular velocity of the disc and the braking torque are assumed constant. The second assumption produces a constant heat flux that is 'smeared out' over the entire rubbing surface, which tends to simplify the thermal transients within the disc material.

Figure 11 shows the disc and calliper assembly temperature variations for lap 15, with the associate RMS errors appearing in Table 6. Of note is the fact that the optimised effective disc thermal capacity is approximately one tenth of the value associated with whole disc. This allows the bulk of the brake disc to heat more slowly than the surface material immediately under the brake pads. As can be seem, both the disc and calliper assembly are heated under braking which occurs between approximately 200 m and 300 m, and between 1250 m and 1500 m. When interpreting these results, one observes that the disc and calliper assembly measurements come from sensors that record the surface temperature at isolated points, while the model produces a temperature that is in some sense representative of each component as a uniformly heated lumped mass.

That said, the model appears to be accurate apart from the steep rises in temperature that occur after the onset of braking into Turn 3. The subsequent cooling of the disc is being well represented by the model. The calliper assembly temperature variations are slow, and are well reproduced by the model. In the case of the left-rear calliper assembly, one sees that minor temperature variations following the onset of braking into Turns 1 and 3.

The optimised convective cooling surfaces used for the front-left brake are shown in Figure 12; the other three brakes behave in qualitatively the same way.

Table 6. Optimised RMS temperature prediction errors for lap 15 measurement data.

Wheel	Disc Temp. Error (C°)	calliper Temp. Error (C°)
Right Front	20.0	0.067
Left Front	24.43	0.327
Right Rear	24.43	0.327
Left Rear	6.47	0.816

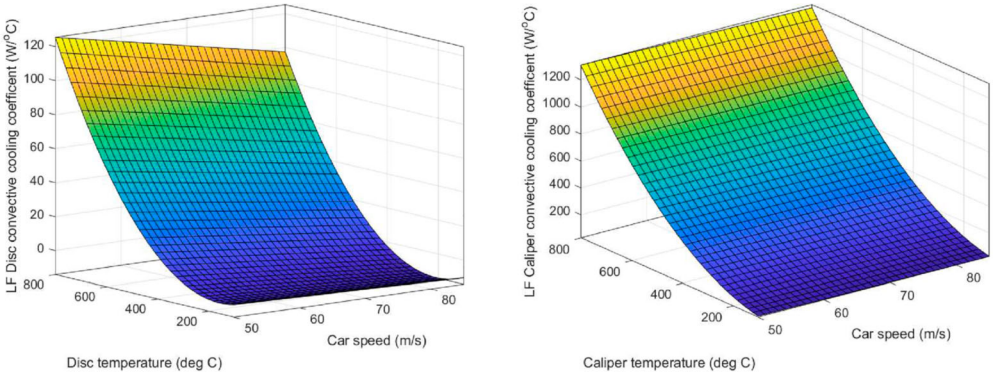

Figure 12. Front-left disc and calliper conductive cooling coefficients as functions of the vehicle speed, and the disc and calliper temperatures.

The optimised parameters indicate that $A^{air}_{disc}\alpha_{disc}(T_d, u_n)$ and $A^{air}_{cal}\alpha_{cal}(T_c, u_n)$ are positive for all T_d, T_c and u_n, that they increase strongly with T_d and T_c, and that they are somewhat less influenced by u_n.

4. Optimal control results

We conclude the paper by showing some of the results generated by an optimal control code that is an extended version of that described in [8]. Extensions include: (i) a NASCAR Gen 7 vehicle parameter set; (ii) Gen 7 tyre model parameters; (iii) an updated suspension model; (iv) a Gen 7 aero map; (v) tyre temperature and wear models; and (vi) a brake system thermal model. The general approach to the aerodynamic modelling is described in [8], but is based on a test dataset that corresponds to a Gen 7 vehicle. The aerodynamic forces and moments are influenced by the vehicle's front and rear ride heights, and the vehicle's roll and side-slip angles. Unlike previous studies, the influence of tyre squash on the aerodynamic forces and moments has been included. The suspension is treated on a one-axle-at-a-time basis and includes the anti-roll bars. The tyre-temperature model describes the tyre carcass and tread temperature variations for each wheel. This model is described in Section 2.1. The tyre wear is described by the wear-rate model given in Section 2.2. The tyre wear and thermal models were introduced into the optimal control studies as a multiplicative correction factor on the tyre forces. That is, for each tyre we have

$$F^c_x = F_x g(t) \int_0^s \mathrm{d}sw(t) \tag{35}$$

$$F^c_y = F_y g(t) \int_0^s \mathrm{d}sw(t), \tag{36}$$

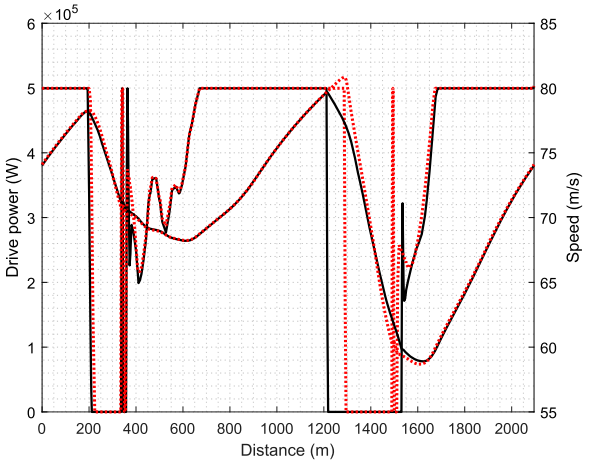

Figure 13. Vehicle speed and engine drive power. The solid lines show the car performance with the disc temperature limit in place and the dotted curves without it.

where F_x^c and F_y^c are the longitudinal and lateral tyre forces corrected for tread temperature and wear (F_x and F_y are the uncorrected values). These forces are degraded as the tread temperatures vary around their optimal values–note that $g(t)\int_0^s \mathrm{d}sw(t) \leq 1$. The degradation of these forces due to accumulated tyre wear is determined by integrating the temperature-sensitive wear-rate function. The grip and wear-rate functions are described in Section 2.

A new temperature-related brake disc and calliper model is also introduced and tested; see Section 3. Given the emphasis of tyre and brake heating influences on the car's performance, the results presented will focus on the tyre tread and carcass temperatures, the tyre wear, and the effect of limiting the front-axle brake disc temperatures. The results relate to testing carried out on the Darlington Speedway.

Wear-related tyre degradation is barely visible in single-lap simulations, but the results highlight how the wear rate varies around the track. Accelerated wear models can be used to study tyre wear with reduced lap numbers. Multi-lap studies can be implemented as multi-phase optimal control problem, with each lap treated as a phase [5]. The effect that disc temperatures changes have on the car's performance comes from a 500°C inequality constraints placed on the front-disc peak temperatures[3]. These results are compared to those obtained without a constraint on the front disc temperatures. The optimal control calculations were performed using GPOPS-II and the Ipopt nonlinear programme solver [37]. The simulated optimal lap times are given by 29.86 s with the disc temperature limit in place, and 29.82 s without it; this constitutes a difference of 40 ms.

Figure 13 shows the speed and engine drive power for the constrained and unconstrained front disc temperature cases; the vehicle speed is shown on the right-hand axis.

In both cases the engine drive shows the *bang-bang* behaviour typically associated with minimum-time optimal control problems. In the brake-disc-temperature limited case, the drive power 'switches' to zero earlier in the entrance to Turn 3, which consequently reduces the car's top speed from 80.8 m/s to 79.7 m/s. This early reduction in engine power is

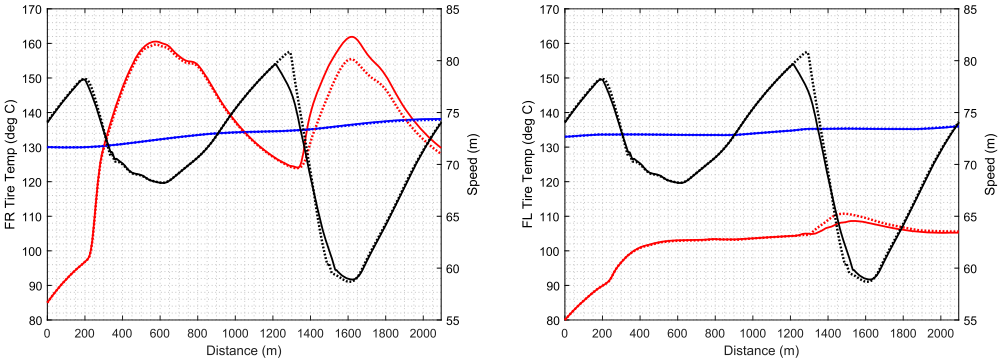

Figure 14. Front-wheel tyre tread and carcass temperatures; the left-hand tyre is on the left, while the right-hand tyre is on the right. The tread temperature is shown in red, while the carcass temperature is in blue. The front disc-temperature-limited case is shown solid.

accompanied by simultaneous early braking that facilitates 'gentler' braking deeper into Turn 3. This gentler braking reduces the rapid increase in front brake disc temperature (particularly the left-front).

Figure 14 shows the behaviour of the front-axle tyre tread and carcass temperatures over a single lap.

The carcass temperatures show a slow marginal increase that persists over multiple laps. The temperature of the lightly-loaded front-left tyre tread increase by approximately 20°C until optimal operating conditions are reached. The more heavily loaded front-right tyre shows much larger tread temperature variations (≈ 75°C) with a rapid increase occurring under braking into Turn 1. The front-right tread temperature then drops by over 30°C as a result of high-speed convective cooling until the car starts to brake into Turn 3. The front-right tread then experiences a second rapid increase in temperature to approximately 160°C. The temperature variations for the front-left tread are significantly smaller due to less onerous loading conditions. The tread temperature increase after 1300 m in the disc-temperature-limited case is primarily due to heavy early braking on the entry to Turn 3. This elevated disc-temperature-limited case temperature is maintained for the remainder of the lap.

Figure 15 shows the behaviour of the rear-axle tyre tread and carcass temperatures over a single lap. The vehicle speed is again shown on the right-hand axis.

If the tyre carcass temperatures are initialised at values that are representative of racing conditions, one observes a gradual steady increase in the carcass temperature in the 5°C to 15°C range. This increase is due primarily to cyclic loading of the carcass and heat conduction from the tread. In contrast, the temperature of the tyre treads varies more rapidly and over a wider range. Both rear-axle tread temperatures start below their optimal operating values and then increase under acceleration over the first 800 m from the start-finish line. These increases are due to high sustained rear-wheel drive torques–primarily for the right-rear wheel. The temperature of the left-hand tread then cools slightly until the entry to Turn 3, when a slow increase occurs under braking. This left-hand tyre tread temperatures drop is the result primarily of convective cooling. A tread temperature of approximately 110° is then maintained for the remainder of the lap. The prolonged braking period in the case of the limited front-disc temperature causes a slight transient increase in the right-rear

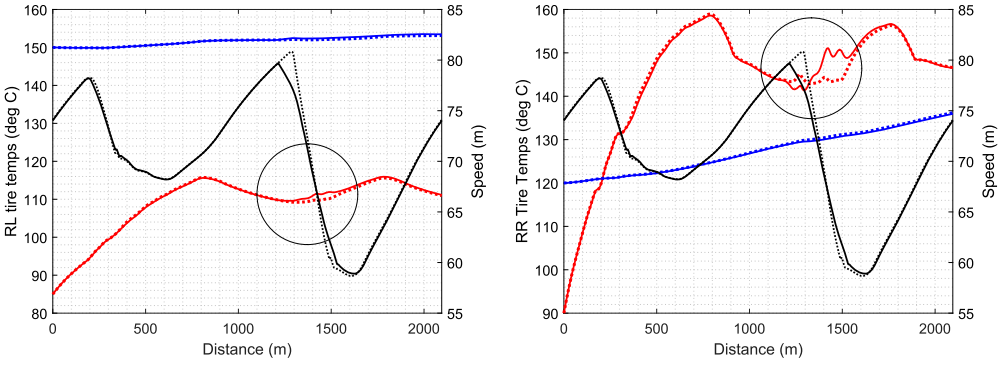

Figure 15. Rear-wheel tyre tread and carcass temperatures; the left-hand tyre is on the left, while the right-hand tyre is on the right. The tread temperature is shown in red, while the carcass temperature is illustrated in blue. The disc-temperature-limit case is shown solid.

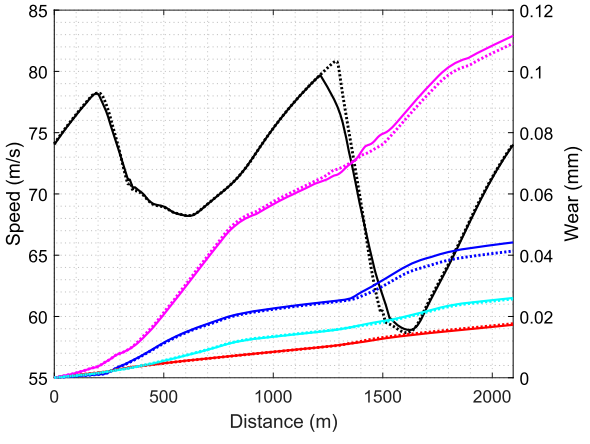

Figure 16. Left axis: Single-lap tyre wear. Right-axis: vehicle speed. The front-right tyre is shown in blue, the front-left in red, the rear-right in magenta, and the left-rear in cyan. The disc-temperature-limit cases are shown solid.

wheel tread temperature. The tread temperatures changes are far more pronounced for the right-rear tread due to the significantly higher drive torque (as compared with the left-rear tyre). Again, the tread cools over the 800 m to 1400 m section in the lead up to Turn 3. The gentler braking in the disc-temperature-limited case causes the tread temperature to cool slightly more than the unlimited disc-temperature case, but there is a short period of higher tread temperature in the disc-temperature-limited case due to a prolonged period of braking. After 1600 m, the tread temperatures in the limited and unlimited disc temperature cases are essentially the same.

Figure 16 shows the wear experienced by each tyre in both the disc-temperature-limited and disc-temperature-unlimited cases.

The lightly-loaded front-left tyre wears relatively slowly and at an almost constant rate, with the disc-temperature limit immaterial. The left-rear tyre wear behaves in much the same way, but with a slightly higher wear rate. The more heavily loaded front-right tyre

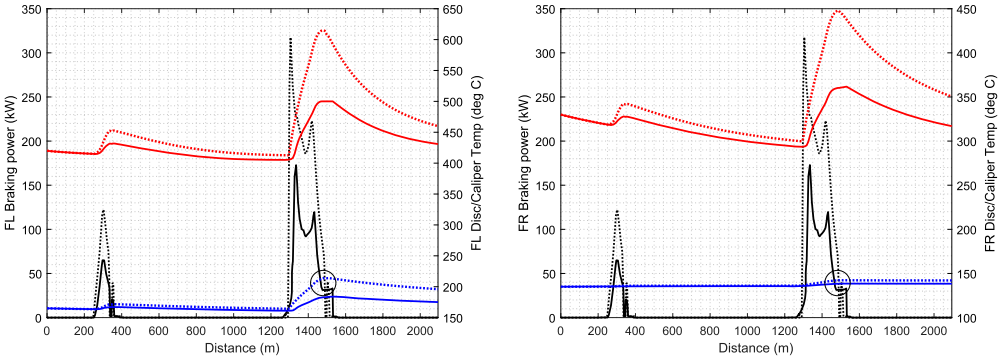

Figure 17. Front-wheel disc and calliper temperatures; the left-hand brake is on the left, while the right-hand brake is on the right. The disc temperature is shown in red, while the calliper temperature is illustrated in blue. The braking powers are shown in black. The disc-temperature-limited case is shown solid.

shows a higher wear rate that increases on the entry to Turn 3. In the case of the active disc temperature limit, the higher wear increase appears to be due to an extended period of braking and the associated increased tread temperature. To see this we refer the reader to Figures 3 and 14. The wear rate of the rear-right tyre is significantly higher than the other three (by a factor of almost three). This difference begins during the acceleration phase towards Turn 1, and is predominantly due to the fact that the rear-right tyre carries the highest normal, longitudinal and lateral tyre loads. The value of tyre-wear modelling stems from the fact that it can predict the wear rate throughout the lap rather than just at the end of a multi-lap test session when tread-depth-measurements are taken.

Figure 17 shows the predicted behaviour of the front brake disc and calliper temperatures. The right-hand axis gives the braking heating power on each wheel, which is of the form given in (26). The braking power represents the conversion of the car's bulk kinetic energy into heat; these heating powers have the potential to achieve values in the hundreds of Kilowatt range [38].

As with the tyre carcass temperatures, the front-axle calliper temperatures maintain reasonably constant values, with both callipers showing a slight increase under braking on the entry to Turn 1. This increase in the calliper temperature is more pronounced in the case of no disc-temperature limit. The observed plateauing in the braking power occurs when the front-left disc temperature constraint is active. When this constraint is active, the braking power is clamped at a value that maintains zero net heat transfer to the front-left disc. Both front-axle discs show rapid and significant temperature increases under braking into Turn 3, with the front-left disc showing an increase of over 200 °, in approximately 5 s (in the unrestricted disc temperature case). When the disc temperature limit is in place this increase reduces to approximately 100 °. Limiting the front-left disc temperature is achieved by reducing the peak braking power, and coming off the throttle earlier into Turn 3. As has already been shown, this strategy involves a sacrifice in top-speed.

5. Conclusions

The thermal management of the brakes and tyres is a crucial element of competitive racing. In order to gain insight into this problem, brake and tyre surface temperature models

were developed and optimised against measured track data. Included also was a tyre wear model that uses the tyre surface temperature and the contact patch frictional power to predict tyre wear. The value of this model is the prediction of the moment-by-moment wear accumulation throughout a racing lap. Pseudospectral optimal control was used to 'drive the car' in order to optimise the tyre friction, manage the brake disc surface temperatures and minimise lap times, whilst also extending the life of the tyres. In the case of the Darlington oval lap studied here, limiting the front disc temperatures has only a minor impact on the optimal lap time. The results suggest that this can be achieved by lifting off the throttle approximately 100 m early on the entrance into Turn 3 (as compared with ignoring the brake temperatures). This change should be accompanied by gentler and prolonged the front-wheel braking. Limiting the front disc temperatures also causes a minor transient increase in the rear-wheel tyre tread temperatures. This is accompanied by an elevated right-front tyre tread temperature on the entry to Turn 3. According to the modelling, limiting the brake disc temperatures results in a minor increase in tyre wear. The methodology presented shows how tyre temperature and wear metrics, and brake thermal models, can be used to understand and manage optimal vehicle race performance.

Notes

1. The power dissipation between the brakes and tyres is anaylsed in [38,39], where a measurement test rig is described. In these papers it is claimed that for the brake and tyre assembly tested, the pneumatic tyre accounts for 30% of the power dissipated by the brake-tyre system as a whole. Referring to the figure below

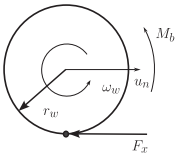

we see that a moment balance on the wheel under braking gives

$$F_x r_w = M_b + J_w \dot{\omega}_w + M_{rr},$$

where M_b is the braking torque, J_w is the spin inertia of the wheel with ω_w its angular velocity, and M_{rr} is the rolling resistance moment. The power dissipated by the braking system is

$$\begin{aligned} \omega_w M_b &= \omega_w \left(F_x r_w - M_{rr} - \omega_w J_w \dot{\omega}_w\right) \\ &= \kappa u_n F_x + u_n F_x - \omega_w M_{rr} - \omega_w J_w \dot{\omega}_w \quad \text{with } \kappa = \frac{r_r \omega_w - u_n}{u_n}. \end{aligned}$$

The first term on the right-hand side is the power associated with the heat dissipation in the tyre tread; see (9). The second term on the right-hand side it the heat dissipated from the brake assembly; see (26). The third term and forth terms represent respectively the dissipations due to rolling resistance and the rate-of-change of the wheel-spin kinetic energy. In this work the wheel deceleration and rolling resistance powers are deemed to be 'small'.
2. These polynomials are sometimes called sums-of-squares polynomials [40], and can be decomposed as $A^{air}_{disc}\alpha_{disc}(T_d, u_n) = \sum_{i=1}^{N} f_i^2(u_n, T_d)$, respectively, $A^{air}_{cal}\alpha_{cal}(T_c, u_n) = \sum_{i=1}^{M} g_i^2(u_n, T_c)$.
3. Brake fade is a loss-of-efficiency phenomenon that is associated with the degradation of composite friction materials at elevated operating temperatures [34]. Brake heating may also lead to thermal distortion that, in turn, produce localised contact areas and the formation of 'hot spots'.

Macroscopic hot spots are a dangerous phenomenon in disc braking systems that can leading to damage and early failure and are areas of high thermal gradient that induce stress cycling within the disc that can lead to cracking. To model these phenomena with proper fidelity, computer models must involve finite-element representation of the heat diffusion Equation (4) [41]. The lumped parameter model used here cannot replicate these deleterious thermal-gradient-related phenomena. For that reason placing an upper bound of 500°C (or any other sensible value) should be seen as a heuristic used to ensure efficient brake disc performance and longevity.

Disclosure statement

No potential conflict of interest was reported by the author(s).

References

[1] Farroni F, Russo M, Russo R, et al. A physical-analytical model for a real-time local grip estimation of tyre rubber in sliding contact with road asperities. Proc Inst Mech Eng, Part D: Journal of Automobile Engineering. 2014 Feb;228(8):955–969. doi: 10.1177/0954407014521402
[2] Farroni F, Sakhnevych A, Timpone F. Physical modelling of tire wear for the analysis of the influence of thermal and frictional effects on vehicle performance. Proc Inst Mech Eng, Part L: Journal of Materials: Design and Applications. 2017 Feb;231(1-2):151–161.
[3] Kelly DP, Sharp RS. Time-optimal control of the race car: influence of a thermodynamic tyre model. Vehicle Syst Dyn. 2012 Apr;50(4):641–662. doi: 10.1080/00423114.2011.622406
[4] Tremlett AJ, Limebeer DJN. Optimal tyre usage for a formula one car. Vehicle Syst Dyn. 2016 Oct;54(10):1448–1473. doi: 10.1080/00423114.2016.1213861
[5] West WJ, Limebeer DJN. Optimal tyre management for a high-performance race car. Vehicle Syst Dyn. 2022;60(1):1–19. doi: 10.1080/00423114.2020.1802047
[6] Limebeer DJN, Massaro M. Dynamics and optimal control of road vehicles. Oxford: Oxford University Press; 2018.
[7] Massaro M, Limebeer D. Minimum-lap-time optimization andsimulation. Vehicle Syst Dyn. 2021;59(7):1069–1113. doi: 10.1080/00423114.2021.1910718
[8] Limebeer DJN, Bastin M, Warren E, et al. Optimal control of a NASCAR-specification race car. Vehicle Syst Dyn. 2022;61(5):1210–1235. doi: 10.1080/00423114.2022.2067573
[9] Farroni F, Giordano D, Russo M, et al. TRT: thermo racing tyre a physical model to predict the tyre temperature distribution. Meccanica. 2014;49(3):707–723. doi: 10.1007/s11012-013-9821-9
[10] Gipser M. Ftire–the tire simulation model for all applications related to vehicle dynamics. Vehicle Syst Dyn. 2007;45:139–151. doi: 10.1080/00423110801899960
[11] Grosch KA. The relation between the friction and visco-elastic properties of rubber. Proc R Soc A. 1963 Jun;274(1356):21–39.
[12] Williams M, Landel R, Ferry F. The temperature dependence of relaxation mechanisms in amorphous polymers and other glass-forming liquids. J Am Chem Soc. 1955;77(14):3701–3707. doi: 10.1021/ja01619a008
[13] Persson BNJ. Theory of rubber friction and contact mechanics. J Chem Phys. 2000;115(8):3840–3861. doi: 10.1063/1.1388626
[14] Schallamach A, Turner DM. The wear of slipping wheels. Wear. 1960;3:1–25. doi: 10.1016/0043-1648(60)90172-1
[15] Grosch KA, Schallamach A. Tyre wear at controlled slip. Wear. 1961;4:356–371. doi: 10.1016/0043-1648(61)90003-5
[16] Muhr AH, Roberts AD. Rubber abrasion and wear. Wear. 1992;158:213–228. doi: 10.1016/0043-1648(92)90040-F
[17] Persson BNJ, Tosatti E. Qualitative theory of rubber friction and wear. J Chem Phys. 2000;112(4):2021–2029. doi: 10.1063/1.480762
[18] Schallamach A. Recent advances in knowledge of rubber friction and tire wear. Rubber Chem Technol. 1968;41(1):209–244. doi: 10.5254/1.3539171

[19] Veirh AG. A review of important factors affecting treadwear. Rubber Chem Technol. 1992;65(3):601–659. doi: 10.5254/1.3538631
[20] Oshinibosi A, Barton D, Brooks P. Optimization of thermal performance and weight of an automotive disc brake for a high performance passenger car. In: EuroBrake 2020.
[21] Cho HJ, Cho CD. A study of thermal and mechanical behaviour for the optimal design of automotive disc brakes. Proc IMechE Part D: J Automobile Engineering. 2008;222:895–915. doi: 10.1243/09544070JAUTO722
[22] Yevtushenko A, Grzes P. Finite element analysis of heat partition in a pad/disc brake system. Numerical Heat Transfer, Part A: Applications. 2011;59(7):521–542. doi: 10.1080/10407782.2011.561098
[23] Talati F, Jalalifar S. Analysis of heat conduction in a disk brake system. Heat Mass Transfer. 2009;45:1047–1059. doi: 10.1007/s00231-009-0476-y
[24] Choi JH, Lee I. Finite element analysis of transient thermoelastic behaviors in disk brakes. Wear. 2004;257:47–58. doi: 10.1016/j.wear.2003.07.008
[25] aus der Wiesche S. Heat transfer from a rotating disk in a parallel air crossflow. Int J Thermal Sci. 2007;46:745–754. doi: 10.1016/j.ijthermalsci.2006.10.013
[26] Sheridan DC, Kutchey JA, Samie F. Approaches to the thermal modeling of disc brakes. SAE Trans. 1988;97:268–283.
[27] Arnold M, Bolay M, Stump O, et al. Numerical efficient thermal network for calculating thebrake disc temperature. J Mech Eng Autom. 2020;10:1–10.
[28] Clark SK, Dodge RN. heat generation in aircraft tires. Comput Struct. 1985;20(1-3):535–544. doi: 10.1016/0045-7949(85)90101-4
[29] Çengel Y, Cimbala J. Fluid mechanics – fundamentals and applications. New York: McGraw-Hill; 2014.
[30] Lechtenboehmer A, Moneypenny HG, Mersch F. A review of polymer interfaces in tyretechnology. British Polymer J. 1990;22:265–301. doi: 10.1002/pi.v22:4
[31] Moore DF. Friction and wear in rubber tyres. Wear. 1980;61:273–282. doi: 10.1016/0043-1648(80)90291-4
[32] Grosch KA. Correlation between road wear of tires and computer road wear simulation usinglaboratory abrasion data. Rubber Chem Technol. 2004;77(5):791–814. doi: 10.5254/1.3547852
[33] Grosch KA. Rubber abrasion and tire wear. Rubber Chem Technol. 2008;81(3):470–505. doi: 10.5254/1.3548216
[34] Cristol-Bulthé A, Desplanques Y, Degallaix G, et al. Mechanical and chemical investigation of the temperature influence on the tribological mechanisms occurring in OMC/cast iron friction contact. Wear. 2008;264:815–825. doi: 10.1016/j.wear.2006.12.080
[35] Tang J, Bryant D, Qi H. A 3D finite element simulation of ventilated brake disc hot spotting. In: Proceedings of the EuroBrake 2016 Conference. Milan: Eurobrake; 2016 Jun. p. 13–15.
[36] Düzgün M. Investigation of thermo-structural behaviors of different ventilation applications on brake discs. J Mech Sci Technol. 2011;26(1):1–6.
[37] Patterson MA, Rao AV. GPOPS-II: A MATLAB software for solving multiple-phase optimal control problems using hp-adaptive Gaussian quadrature collocation methods and sparse nonlinear programming. ACM Trans Math Softw. 2014 Oct;41(1):1–37. doi: 10.1145/2558904
[38] Cantoni C, Gobbi M, Mastinu G, et al. Brake and pneumatic wheel performance assessment–A new test rig. Measurement. 2020;150:107042. doi: 10.1016/j.measurement.2019.107042
[39] Cantoni C, Gobbi M, Mastinu G, et al. Tire and brake interaction – a new test rig to study wheel locking. SAE Technical Paper 2021-01-0972, 2021.
[40] Packard A, Topcu U, Seiler P, et al. Help on SOS. IEEE Control Syst Mag. 2010;30(4):18–23. doi: 10.1109/MCS.2010.937045
[41] Panier S, Dufrénoy P, Weichert D. An experimental investigation of hot spots in railway disc brakes. Wear. 2004;256:764–773. doi: 10.1016/S0043-1648(03)00459-9